2018 26th Mediterranean Conference on Control and Automation (MED)
Zadar, Croatia, June 19-22, 2018

Geometric Surface-Based Tracking Control of a Quadrotor UAV for aggressive maneuvers

Michalis Ramp[1] and Evangelos Papadopoulos[2], *Senior Member, IEEE*

***Abstract*— New quadrotor UAV control algorithms are developed, based on nonlinear surfaces composed of tracking errors that evolve directly on the nonlinear configuration manifold, thus inherently including in the control design the nonlinear characteristics of the SE(3) configuration space. In particular, geometric surface-based controllers are developed and are shown, through rigorous stability proofs, to have desirable almost global closed loop properties. For the first time in regards to the geometric literature, a region of attraction independent of the position error is identified and its effects are analyzed. The effectiveness of the proposed 'surface based' controllers are illustrated by simulations of aggressive maneuvers in the presence of disturbances and motor saturation.**

I. Introduction

Quadrotor unmanned aerial vehicles are characterized by a simple mechanical structure comprised of two pairs of counter rotating outrunner motors where each one is driving a dedicated propeller, resulting in a platform with high thrust-to-weight ratio, able to achieve vertical takeoff and landing (VTOL) maneuvers and operate in a broad spectrum of flight scenarios. Quadrotors have good flight endurance characteristics and acceptable payload transporting potential for a plethora of applications. Although the quadrotor UAV has six degrees of freedom, it is underactuated since it has only four inputs and can only track four commands or less.

A plethora of theoretical and experimental works regarding quadrotors exist including results demonstrating aerobatic maneuvers [1], decentralized collision avoidance for multiple quadrotors [2], safe passage schemes satisfying constraints on velocities, accelerations, and inputs [3], backsteping [4], and hybrid global/robust controllers [5], [6], [7].

In this paper, a geometric nonlinear control system (GNCS) for a quadrotor UAV is developed directly on the special Euclidean group, thus inherently entailing in the control design the characteristics of the nonlinear configuration manifold, and avoiding singularities and ambiguities associated with minimal attitude representations. The key contributions of this work are: (a) An attitude and a position controller is developed based on nonlinear surfaces composed by tracking errors that evolve directly on the nonlinear configuration manifold. These controllers allow for precision pose tracking by tuning three gains per controller. (b) In contrast to other GNCSs such as [1], [8] - [12], rigorous stability proofs are developed and regions of attraction both with and without restrictions on the initial position/velocity error are identified, thus introducing simplicity in trajectory design. The proposed strategies are validated in simulation in the presence of motor saturation and wind disturbances.

II. Quadrotor Kinetics Model

The quadrotor studied is comprised by two pairs of counter rotating out-runner motors. Each motor drives a dedicated propeller and generates thrust and torque normal to the plane produced by the centers of mass (CM) of the four rotors. An inertial reference frame $\mathrm{I}_R\{\mathbf{E}_1, \mathbf{E}_2, \mathbf{E}_3\}$ and a body-fixed frame $\mathrm{I}_b\{\mathbf{e}_1, \mathbf{e}_2, \mathbf{e}_3\}$ are employed with the origin of the latter to be located at the quadrotor CM, which belongs to the four rotor CM plane. Vectors $\mathbf{e}_1$ and $\mathbf{e}_2$ are co-linear with the two quadrotor legs. The following apply throughout the paper. The actual control input is the thrust of each propeller, which is co-linear with $\mathbf{e}_3$. The first and third propellers generate positive thrust when rotating clockwise, while the second and fourth propellers generate positive thrust when rotating counterclockwise. The collective thrust is denoted by $f = \sum_{i=1}^{4} f_i \in \mathbb{R}$, where f_i and other system variables are described in Table I.

TABLE I: Definitions of variables.

$\mathbf{x} \in \mathbb{R}^3$	Quadrotor CM position in I_R
$\mathbf{v} \in \mathbb{R}^3$	Quadrotor CM velocity in I_R
${}^b\boldsymbol{\omega} \in \mathbb{R}^3$	Angular velocity of the quadrotor wrt. I_R in I_b
$\mathbf{R} \in \mathrm{SO}(3)$	Rotation matrix from $\mathbf{I}_b$ to $\mathbf{I}_R$ frame
${}^b\mathbf{u} \in \mathbb{R}^3$	Control moment ${}^b\mathbf{u}=[{}^bu_1; {}^bu_2; {}^bu_3]$ in I_b
$f_i \in \mathbb{R}$	Force produced by the i-th propeller along $\mathbf{e}_3$
$b_T \in \mathbb{R}^+$	Torque coefficient
$g \in \mathbb{R}$	Gravity constant
$d \in \mathbb{R}^+$	Distance between system CM and each motor axis
$\mathbf{J} \in \mathbb{R}^{3\times 3}$	Inertial matrix (IM) of the quadrotor in I_b
$m \in \mathbb{R}$	Quadrotor total mass
$\lambda_{min,max}(.)$	Minimum, maximum eigenvalue of (.) respectively

The motor torques, $\boldsymbol{\tau}_i$, corresponding to each propeller are assumed to be proportional to thrust,

$$\boldsymbol{\tau}_i = (-1)^i b_T f_i \mathbf{e}_3,\ i = 1, .., 4 \tag{1}$$

where the $(-1)^i$ term connects each propeller with the correct rotation direction. The control inputs include the collective thrust, f, and moment, ${}^b\mathbf{u}$, given by,

$$\begin{bmatrix} f \\ {}^b\mathbf{u} \end{bmatrix} = \begin{bmatrix} 1 & 1 & 1 & 1 \\ 0 & d & 0 & -d \\ -d & 0 & d & 0 \\ -b_T & b_T & -b_T & b_T \end{bmatrix} \mathbf{F},\ \mathbf{F} = \begin{bmatrix} f_1 \\ f_2 \\ f_3 \\ f_4 \end{bmatrix} \tag{2}$$

with $\mathbf{F} \in \mathbb{R}^4$ the thrust vector, and the 4×4 matrix to be of full rank for $d, b_T \in \mathbb{R}^+$ and thus always invertible.

[1]M. Ramp is with the Department of Mechanical Engineering, National Technical University of Athens, (NTUA) 15780 Athens, Greece. rampmich@mail.ntua.gr

[2]E. Papadopoulos is with the Department of Mechanical Engineering, NTUA, 15780 Athens (tel: +30-210-772-1440; fax: +30-210-772-1455). egpapado@central.ntua.gr

The spatial configuration of the quadrotor UAV is described by the quadrotor attitude and the location of its center of mass, both with respect to $\mathbf{I}_R$. The configuration manifold is SE(3)=$\mathbb{R}^3 \times$ SO(3), the special Euclidean group. The equations of motion of the quadrotor are given by,

$$\dot{\mathbf{x}} = \mathbf{v}$$

$$m\dot{\mathbf{v}} = -mg\mathbf{E}_3 + \mathbf{R}f\mathbf{e}_3 + \boldsymbol{\delta}_x \quad (3)$$

$$\mathbf{J}^b\dot{\boldsymbol{\omega}} = {}^b\mathbf{u} - {}^b\boldsymbol{\omega} \times \mathbf{J}^b\boldsymbol{\omega} + \boldsymbol{\delta}_R \quad (4)$$

$$\dot{\mathbf{R}} = \mathbf{R}S({}^b\boldsymbol{\omega}) \quad (5)$$

where $\boldsymbol{\delta}_x$, $\boldsymbol{\delta}_R$ are disturbance terms and $S(.) : \mathbb{R}^3 \rightarrow \mathfrak{so}(3)$ is the cross product map given by,

$$S(\mathbf{r}){=}[0, -r_3, r_2; r_3, 0, -r_1; -r_2, r_1, 0], S^{-1}(S(\mathbf{r})){=}\mathbf{r} \quad (6)$$

III. Quadrotor Tracking Controls

Given the underactuated nature of quadrotors, in this paper two flight modes are considered:

- *Attitude Control Mode*: The controller achieves tracking for the attitude of the quadrotor UAV.
- *Position Control Mode*: The controller achieves tracking for the quadrotor CM position and a pointing attitude associated with the quadrotor yaw.

Using these flight modes in suitable successions, a quadrotor can perform a complex flight maneuver. Moreover it will be shown that each mode has stability properties that allow the safe switching between flight modes (end of Section III).

A. Attitude Control Mode (ACM)

A controller to track a sufficiently smooth attitude $\mathbf{R}_d(t)$ is developed, under the assumption that $\boldsymbol{\delta}_R{=}0_{3\times1}$.

1) Attitude tracking errors: For a given tracking command ($\mathbf{R}_d, {}^b\boldsymbol{\omega}_d$) and current state ($\mathbf{R}, {}^b\boldsymbol{\omega}$), two sets of tracking errors are considered. Each set consists of an *attitude error function* Ψ:SO(3)×SO(3)→$\mathbb{R}$, and an *attitude error vector* $\mathbf{e}_R \in \mathbb{R}^3$, defined as follows. The first set is, [9]:

$$\Psi(\mathbf{R}, \mathbf{R}_d) = \frac{1}{2}tr[\mathbf{I} - \mathbf{R}_d^T\mathbf{R}] \geq 0 \quad (7)$$

$$\mathbf{e}_R(\mathbf{R}, \mathbf{R}_d) = \frac{1}{2}S^{-1}(\mathbf{R}_d^T\mathbf{R} - \mathbf{R}^T\mathbf{R}_d) \quad (8)$$

with $tr[.]$ the trace function. The second according to [13]:

$$\Psi(\mathbf{R}, \mathbf{R}_d){=}2 - \sqrt{1 + tr[\mathbf{R}_d^T\mathbf{R}]} \geq 0 \quad (9)$$

$$\mathbf{e}_R(\mathbf{R}, \mathbf{R}_d){=}\frac{1}{2}S^{-1}(\mathbf{R}_d^T\mathbf{R}{-}\mathbf{R}^T\mathbf{R}_d)(1{+}tr[\mathbf{R}_d^T\mathbf{R}])^{-\frac{1}{2}} \quad (10)$$

Both (7), (9) yield the angular velocity error vector, $\mathbf{e}_\omega{\in}\mathbb{R}^3$,

$$\mathbf{e}_\omega(\mathbf{R}, {}^b\boldsymbol{\omega}, \mathbf{R}_d, {}^b\boldsymbol{\omega}_d) = {}^b\boldsymbol{\omega} - \mathbf{R}^T\mathbf{R}_d{}^b\boldsymbol{\omega}_d \quad (11)$$

For the ACM, the controller is designed to be compatible with both sets of $\mathbf{e}_R$. This is because the first set given by $\{(7), (8)\}$ bestows excellent tracking properties to the controller if the orientation tracking error remains less than 90^o wrt. an axis-angle rotation; however for larger orientation errors, the magnitude of the attitude error vector, (8), is not proportional to the orientation error and results to deteriorating performance as the state approaches the antipodal equilibrium (see [13] for more details). In contrast to this, the second set $\{(9), (10)\}$ does not suffer from this problem but is marginally outperformed by the first set if the attitude error is less than 90^o. Thus depending on the flight conditions, the user can choose which set of attitude tracking errors to use.

The maximum attitude error, that of 180^o wrt. an axis-angle rotation between $\mathbf{R}$ and $\mathbf{R}_d$, occurs when the rotation matrices are antipodal; then (7) or (9) yield $\Psi(\mathbf{R}, \mathbf{R}_d)$=2, i.e. 100% error. If $\mathbf{R}$, $\mathbf{R}_d$, express the same attitude i.e., $\mathbf{R}$=$\mathbf{R}_d$, then $\Psi(\mathbf{R}, \mathbf{R}_d)$=0, i.e. 0% error. Properties about (7)-(11), and their assosiated error dynamics are given in [9], [13].

2) Attitude tracking controller: A controller is developed stabilizing $\mathbf{e}_R$, $\mathbf{e}_\omega$, to zero exponentially, almost globally under the assumption that $\boldsymbol{\delta}_R = 0_{3\times1}$.

Proposition 3. For $\eta, k_R, k_\omega \in \mathbb{R}^+$, with,

$$\eta > k_R/{k_\omega}^2 \quad (12)$$

and initial conditions satisfying,

$$\Psi(\mathbf{R}(0), \mathbf{R}_d(0)) < 2 \quad (13)$$

$$\|\mathbf{e}_\omega(0)\|^2 < 2\eta k_R \left(2 - \Psi(\mathbf{R}(0), \mathbf{R}_d(0))\right) \quad (14)$$

and for a desired arbitrary smooth attitude $\mathbf{R}_d(t){\in}$SO(3) in,

$$L_2 = \{(\mathbf{R}, \mathbf{R}_d) \in \text{SO(3)} \times \text{SO(3)} | \Psi(\mathbf{R}, \mathbf{R}_d) < 2\} \quad (15)$$

then, under the assumption of perfect parameter knowledge, we propose the following nonlinear surface-based controller,

$${}^b\mathbf{u} = {}^b\boldsymbol{\omega} \times \mathbf{J}^b\boldsymbol{\omega} - \mathbf{J}\left(\frac{k_R}{k_\omega}\dot{\mathbf{e}}_R + \mathbf{a}_d + \eta\mathbf{s}_R\right) \quad (16a)$$

$$\mathbf{a}_d = S({}^b\boldsymbol{\omega})\mathbf{R}^T\mathbf{R}_d{}^b\boldsymbol{\omega}_d - \mathbf{R}^T\mathbf{R}_d{}^b\dot{\boldsymbol{\omega}}_d \quad (16b)$$

$$\mathbf{s}_R = k_R\mathbf{e}_R + k_\omega\mathbf{e}_\omega \quad (16c)$$

where $\dot{\mathbf{e}}_R$, if the $\{(7), (8)\}$ set is used, it is given by

$$\dot{\mathbf{e}}_R = \frac{1}{2}\{tr[\mathbf{R}^T\mathbf{R}_d]\mathbf{I} - \mathbf{R}^T\mathbf{R}_d\}\mathbf{e}_\omega \quad (17)$$

while if the $\{(9), (10)\}$ set is used, $\dot{\mathbf{e}}_R$ is given by,

$$\dot{\mathbf{e}}_R = \frac{\{tr[\mathbf{R}^T\mathbf{R}_d]\mathbf{I} - \mathbf{R}^T\mathbf{R}_d + 2\mathbf{e}_R\mathbf{e}_R^T\}}{2\sqrt{1 + tr[\mathbf{R}_d^T\mathbf{R}]}}\mathbf{e}_\omega \quad (18)$$

Then, the zero equilibrium of the quadrotor closed loop attitude tracking error $(\mathbf{e}_R, \mathbf{e}_\omega) = (\mathbf{0}, \mathbf{0})$ is almost globally exponentially stable; moreover $\exists\mu, \tau > 0$ such that

$$\Psi(\mathbf{R}, \mathbf{R}_d) < min\{2, \mu e^{-\tau t}\} \quad (19)$$

Proof. Due to space limitations see [14], Appendix B.

The convergence properties introduced by the surface $\mathbf{s}_R$ are analyzed at the end of Section III. The initial angular velocity can be arbitrarily large by using sufficiently large gains. The region of attraction given by (13)-(14) ensures that $\mathbf{R}_d$ is not antipodal to $\mathbf{R}$, because the topology of SO(3) prohibits the design of a smooth global controller, [15]. Thus exponential stability is guaranteed almost globally.

Because (16a) is developed directly on SO(3), it avoids singularities associated with minimum attitude representations and it can control the attitude dynamics of any rigid body and not only quadrotor systems. Attitude tracking does not depend on f, the ACM is more suited for short durations of time. The thrust magnitude can be selected to achieve any additional objective compatible with the attitude tracking task. An example is tracking a desired altitude [1]. Despite developing (16a) under the assumption that $\boldsymbol{\delta}_R=0_{3\times1}$, its robustness properties will be tested in simulation considering motor saturation and wind disturbances.

B. Position Control Mode (PCM)

Under the assumption that $\boldsymbol{\delta}_x=0_{3\times1}$, a controller is developed for the position dynamics of the quadrotor, stabilizing the tracking errors to zero asymptotically, almost globally.

1) Position tracking errors: For an arbitrary smooth position tracking instruction $\mathbf{x}_d\in\mathbb{R}^3$, the tracking errors are,

$$\mathbf{e}_x = \mathbf{x} - \mathbf{x}_d,\ \mathbf{e}_v = \mathbf{v} - \dot{\mathbf{x}}_d \tag{20}$$

For $k_x, k_v\in\mathbb{R}^+$ the position surface is defined as,

$$\mathbf{s}_x = k_x\mathbf{e}_x + k_v\mathbf{e}_v \tag{21}$$

In the PCM, the attitude dynamics must be compatible with the desired position tracking. This results in the definition of a position-induced attitude matrix, $\mathbf{R}_x(t)\in\mathrm{SO(3)}$, for use as an attitude command. To define this matrix, first the desired thrust direction of the quadrotor, $\mathbf{e}_{3_x}$, is computed,

$$\mathbf{e}_{3_x}=\frac{mg\mathbf{E}_3 - m\frac{k_x}{k_v}\mathbf{e}_v - a\mathbf{s}_x + m\ddot{\mathbf{x}}_d}{\|mg\mathbf{E}_3 - m\frac{k_x}{k_v}\mathbf{e}_v - a\mathbf{s}_x + m\ddot{\mathbf{x}}_d\|} \in \mathrm{S}^2, a\in\mathbb{R}^+ \tag{22}$$

where it is assumed that by selecting $\mathbf{x}_d$, $\dot{\mathbf{x}}_d$, $\ddot{\mathbf{x}}_d$ hereafter,

$$\|mg\mathbf{E}_3 - m\frac{k_x}{k_v}\mathbf{e}_v - a\mathbf{s}_x + m\ddot{\mathbf{x}}_d\| > 0$$

i.e. the set of admissible trajectories result to a physical thrust direction. Secondly, a desired yaw direction $\mathbf{e}_{1_d}\in\mathrm{S}^2$ of the $\mathbf{e}_1$ body-fixed axis of the quadrotor is defined, so that $\mathbf{e}_{1_d}\nparallel\mathbf{e}_{3_x}$. This is used to find the position-induced heading, $\mathbf{e}_{1_h}$, [8],

$$\mathbf{e}_{1_h} = ((\mathbf{e}_{3_x}\times\mathbf{e}_{1_d})\times\mathbf{e}_{3_x})/\|(\mathbf{e}_{3_x}\times\mathbf{e}_{1_d})\times\mathbf{e}_{3_x}\|$$

The position related attitude $\mathbf{R}_x(t)\in\mathrm{SO(3)}$, ${}^b\boldsymbol{\omega}_x(t)\in\mathbb{R}^{3\times1}$ is,

$$\mathbf{R}_x=\left[\mathbf{e}_{1_h}, \frac{\mathbf{e}_{3_x}\times\mathbf{e}_{1_h}}{\|\mathbf{e}_{3_x}\times\mathbf{e}_{1_h}\|}, \mathbf{e}_{3_x}\right],\ {}^b\boldsymbol{\omega}_x=S^{-1}(\mathbf{R}_x^T\dot{\mathbf{R}}_x) \tag{23}$$

The attitude dynamics are guided to follow $\mathbf{R}_x(t)$, ${}^b\boldsymbol{\omega}_x(t)$.

2) Position tracking controller: Assuming that $\boldsymbol{\delta}_x=0_{3\times1}$, a control system is developed for the position dynamics of the quadrotor, achieving almost global asymptotic stabilization of ($\mathbf{e}_x$,$\mathbf{e}_v$,$\mathbf{e}_R$,$\mathbf{e}_\omega$) to zero through the action/effect of the soon to be introduced Propositions 4 and 5.

For a sufficiently smooth yaw pointing direction $\mathbf{e}_{1_d}(t)\in\mathrm{S}^2$, and a sufficiently smooth position tracking instruction $\mathbf{x}_d(t)\in\mathbb{R}^3$ the following position controller is defined,

$$f(\mathbf{x}_d,\dot{\mathbf{x}}_d,\ddot{\mathbf{x}}_d)=(mg\mathbf{E}_3-m\frac{k_x}{k_v}\mathbf{e}_v-a\mathbf{s}_x+m\ddot{\mathbf{x}}_d)^T\mathbf{R}\mathbf{e}_3 \tag{24a}$$

$${}^b\mathbf{u}(\mathbf{R}_x,{}^b\boldsymbol{\omega}_x)={}^b\boldsymbol{\omega}\times\mathbf{J}{}^b\boldsymbol{\omega}-\mathbf{J}\left(\frac{k_R}{k_\omega}\dot{\mathbf{e}}_{R_x}+\mathbf{a}_{d_x}+\eta\mathbf{s}_{R_x}\right) \tag{24b}$$

where $\mathbf{a}_{d_x}$, $\mathbf{s}_{R_x}$, $\dot{\mathbf{e}}_{R_x}$, are given by (16b)-(18) and the desired attitude matrix that is used in (24) is given by (23).

The use of nonlinear surfaces resulted to the thrust feedback expression, (24a), which includes three gains; yet Eq. (24a) can be scaled to a PD form as in [1]. However, since (24a) is paired with the newly developed attitude controller (24b), it forms a new PCM controller of improved closed loop response wrt. [1] and allows finer tuning, see Sect. IV.

The closed loop system defined by (3)-(5) under the action of (24a)-(24b) is shown to achieve almost global asymptotic stabilization of ($\mathbf{e}_x$,$\mathbf{e}_v$,$\mathbf{e}_R$,$\mathbf{e}_\omega$) to the zero equilibrium by the combined action of Propositions 4 and 5. Specifically (24b) drives $\mathbf{R}(t)$ to asymptotically track $\mathbf{R}_x(t)$ and combined with (24a), asymptotic position tracking is achieved. The first result of exponential stability for a sub-domain of the quadrotor closed loop position dynamics is presented next.

Proposition 4. Considering the controllers in (24a), (24b) and for initial conditions in the domain,

$$D_x = \{(\mathbf{e}_x,\mathbf{e}_v,\mathbf{e}_R,\mathbf{e}_\omega)\in\mathbb{R}^3\times\mathbb{R}^3\times\mathbb{R}^3\times\mathbb{R}^3 | \\ \Psi(\mathbf{R}(0),\mathbf{R}_x(0)) < \psi_p < 1\} \tag{25}$$

and for $\ddot{\mathbf{x}}_d\in\mathbb{R}^{3\times1}$, $B\in\mathbb{R}^+$ such that the following holds,

$$\|mg\mathbf{E}_3 + m\ddot{\mathbf{x}}_d\| \le B \tag{26}$$

We define $\boldsymbol{\Pi}_1,\boldsymbol{\Pi}_2\in\mathbb{R}^{2\times2}$ as,

$$\boldsymbol{\Pi}_1=\begin{bmatrix} ak_x^2(1-\theta) & -ak_xk_v\theta-\frac{mk_x^2\theta}{2k_v} \\ -ak_xk_v\theta-\frac{mk_x^2\theta}{2k_v} & ak_v^2-\theta(mk_x+ak_v^2)\end{bmatrix},$$

$$\boldsymbol{\Pi}_2 = \begin{bmatrix} Bk_x & 0 \\ Bk_v & 0\end{bmatrix} \tag{27}$$

where $\theta < \theta_{max}\in\mathbb{R}^+$ and θ_{max} is given by,

$$\theta_{max} = \min\{\frac{ak_v^2}{ak_v^2+mk_x}, \delta_1+\delta_2\}, \tag{28}$$

$$\delta_1 = 2\frac{k_v^2\sqrt{4k_x^4k_v^4a^4+4k_x^5k_v^2a^3m+2k_x^6m^2a^2}}{k_x^4m^2}$$

$$\delta_2 = -4\frac{a^2k_v^4}{m^2k_x^2}-2\frac{ak_v^2}{mk_x}$$

If $\{(7),(8)\}$ is used, the attitude error bound, ψ_p, satisfies,

$$\theta_{max} = \sqrt{\psi_p(2-\psi_p)}$$

while if the set $\{(9),(10)\}$ is used, ψ_p satisfies,

$$\theta_{max} = \sqrt{\psi_p(1-\frac{\psi_p}{4})}$$

In conjunction with suitable gains $\eta, k_R, k_\omega\in\mathbb{R}^+$, such that,

$$\lambda_{min}(\mathbf{W}_3) > \frac{\|\boldsymbol{\Pi}_2\|^2}{4\eta\lambda_{min}(\boldsymbol{\Pi}_1)}, \mathbf{W}_3 = \begin{bmatrix} k_R^2 & 0 \\ 0 & k_\omega^2\end{bmatrix} \tag{29}$$

then the zero equilibrium of the closed loop errors $(\mathbf{e}_x,\mathbf{e}_v,\mathbf{e}_R,\mathbf{e}_\omega)$ is exponentially stable in the domain given by (25). A region of attraction is identified by (25), (28), and

$$\|\mathbf{e}_\omega(0)\|^2 < 2\eta k_R\left(\psi_p - \Psi(\mathbf{R}(0),\mathbf{R}_x(0))\right) \tag{30}$$

Proof. Due to space limitations see [14], Appendix C.

Proposition 4 requires that the norm of the initial attitude error is less than θ_{max} to achieve exponential stability (the upper bound of θ, (28), depends solely on the control gains and the quadrotor mass). This corresponds to a reduced region of attraction in comparison to the regions in [1], [8] - [12], because no restriction on the initial position/velocity error was applied during the stability proof. This approach is new, wrt. the geometric literature, offering the advantage of simplifying trajectory design. The region of attraction in other geometric treatments includes bounds on the initial position or velocity (see [1], [8] - [12]) meaning that the trajectory should comply to the position/velocity bounds and also to the attitude bound, a more involved task.

If a user prefers a larger basin of exponential stability, this can be achieved by introducing bounds on the initial position/velocity (due to space see [14], Appendix C, Section (f)). Then two new regions of attraction are produced involving larger initial attitude errors, given by (30) and,

$$\Psi(\mathbf{R}(0), \mathbf{R}_x(0)) < \psi_p < 1, \|\mathbf{e}_{x/v}(0)\| < e_{x/v_{max}} \quad (31)$$

$$\theta < \theta_{max} = \min\{\frac{ak_v^2}{ak_v^2 + mk_x}\} \quad (32)$$

where the second inequality in (31) denotes either a bound on the initial position error, $e_{x_{max}}$, or a bound on the initial velocity error, $e_{v_{max}}$, but not on both (due to space see [14], Appendix C, Section (f) for more details and expressions regarding Π_1, Π_2, that comply with (29)). Depending on user preference, the trajectory design procedure can be realized using either one of the three regions of attraction ($\{(25), (28), (30)\}$, $\{(30), (31), (32)\}$ using $e_{x_{max}}$ and $\{(30), (31), (32)\}$ using $e_{v_{max}}$) guiding us to favorable conditions for switching between flight modes. For completeness, all three regions of exponential stability were derived; however this work focuses on the region $\{(25), (28), (30)\}$.

Finally, the next proposition shows that the PCM closed-loop system is almost globaly exponentialy attractive. This compensates for the reduced position/velocity free region of attraction and introduces greater freedom to the user in regards to control objectives, since the region of attraction does not depend explicitly on the initial position/velocity error. If the quadrotor initial states are outside of (25), with respect to the initial attitude, Prop. 3 still applies due to the action of (24b). Thus the attitude state enters (25) in finite time t^* and the results of Prop. 4 take effect. The result regarding the PCM is stated next.

Proposition 5. For initial conditions satisfying (14), and

$$\psi_p \leq \Psi(\mathbf{R}(0), \mathbf{R}_x(0)) < 2 \quad (33)$$

and a uniformly bounded desired acceleration (26), the control (24), renders the zero equilibrium of $(\mathbf{e}_x, \mathbf{e}_v, \mathbf{e}_R, \mathbf{e}_\omega)$ almost globally exponentially attractive.

Proof of Proposition 5. See Prop. 4 in [8] but apply (24a).

Prop. 5 shows that during the finite time that it takes for the attitude states to enter the region of attraction for exponential stability (25), (30), the position errors remain bounded. The region of exponential attractiveness given by (33) ensures that $\mathbf{R}_x(t)$ is not antipodal to $\mathbf{R}(t)$. Thus the zero equilibrium is almost globally exponentially attractive.

For both control modes Section III-A (III-B), through the utilization of the nonlinear surfaces $\mathbf{s}_R$, $(\mathbf{s}_x)$, the dynamics of the system are altered, by influencing the convergence to the zero equilibrium via three gains per surface. Using the gains η, (a), the reaching time to the surface is affected, by penalizing the combined surface error, while the gains $k_R, k_\omega, (k_x, k_v)$, affect the convergence time when on/near the surface by penalizing independently the attitude, angular velocity, (position, translational velocity), errors. This is showcased in Fig. 1, showing responses of an attitude maneuver (Fig. 1a), and a position maneuver (Fig. 1b). In both cases, the simulations are repeated using larger gains η, (a), resulting in faster reaching times, see black solid lines in Fig. 1a,1b. In Fig. 1a, by doubling η, the reaching time from $t_{\mathbf{s}_R}$=0.169 improves to $t_{\mathbf{s}_R}$=0.099. In Fig. 1b, by increasing a by four, the reaching time from $t_{\mathbf{s}_x}$=1.999 improves to $t_{\mathbf{s}_x}$=0.569. Thus, the strict algebraic relation to the gains imposed by the proposed controller design, introduces "sliding like" closed-loop dynamics, see caption in Fig. 1, and allows for finer control on the convergence rate to the zero equilibrium by using the insights gained by the Lyapunov analysis. Also the sliding behavior is achieved without the signum function; thus chattering is avoided.

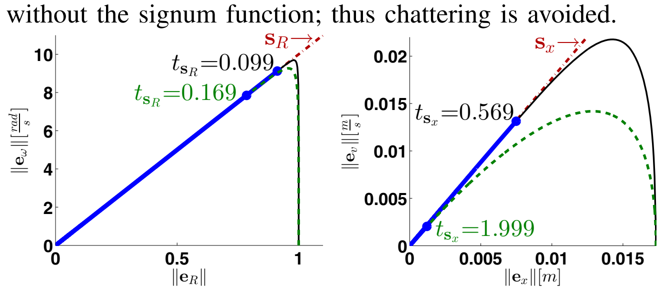

(a) (b)

Fig. 1: Sliding behavior produced by, (16a), ((24a), (24b)) using $\{(9), (10)\}$. (1a) Convergence to $\mathbf{s}_R$ for a step of 179.9999^o. (1b) Convergence to $\mathbf{s}_x$ for a position step to $\mathbf{x}_d$=$[1; 1; 1]cm$. The black and dashed green lines indicate the reaching phase to $\mathbf{s}_{R,x}$ followed by sliding behavior indicated by blue lines. The black lines indicate usage of higher sliding gains η, a. The reaching times, $t_{\mathbf{s}_{R,x}}$, are colored accordingly.

Due to the combined action of (24a) with (24b) it was possible to identify, for the first time wrt. the geometric literature, a region of attraction *independent* of the initial position/velocity error. This is a new development in regards to the geometric literature. Also the developed expression, (24a), with the third gain allows for more intuitive tuning thus offering further refinement of the closed loop response.

Concluding, by the combined action of Prop. 4 and 5, asymptotic almost global stabilization of ($\mathbf{e}_x$,$\mathbf{e}_v$,$\mathbf{e}_R$,$\mathbf{e}_\omega$) to zero is achieved. Since both flight modes are almost global, the closed loop system is robust to switching between flight modes. The only consideration in respect to trajectory planning is that the desired trajectory must agree with (13)-(14). Despite developing (24) under the assumption that $\boldsymbol{\delta}_x$=$0_{3\times1}$, its robustness properties will be tested in simulation in the presence of motor saturation and wind disturbances.

IV. Results

The effectiveness of the developed GNCS is verified through simulations. First by a comparison with [1], to verify the claims of Section III-B.2 in regards to the collective thrust (24a), followed by an aggressive recovery/trajectory tracking maneuver in the presence of motor saturations and noise to test the effectiveness and robustness of the developed GNCS.

To analyze GNCSs of different structure, a criterion is needed for a commensurate comparison. Thus the Root-

Mean-Square (RMS) of the thrusts is used as a criterion,

$$f_{RMS}(t) = \sqrt{\frac{1}{t}\int_0^t \sum_1^4 [f_i(t)]^2 d\tau} \qquad (34)$$

Using (34) we calculate the RMS control effort difference,

$$\Delta f_{_{RMS}}(t) = f_{_{RMS}}^{developed}(t) - f_{_{RMS}}^{benchmark}(t) \qquad (35)$$

and tune our developed GNCS such that (35) is negative at all times so that the benchmark controller has equal or larger control authority. By comparing the controller performance, if the developed GNCS produces the least error with *less control effort* it is deemed superior. The system parameters were obtained from the quadrotor described in [16]:

$$\mathbf{J} = [0.0181, 0, 0; 0, 0.0196, 0; 0, 0, 0.0273]\ kg\, m^2$$

$$m = 1.225\ kg, d = 0.23\ m, b_T = 0.0121\ m$$

and the motor thrust limitations, see [16], are given by:

$$f_{i,min} = 0[\text{N}], f_{i,max} = 6.9939[\text{N}]$$

The wind profile shown in Fig. 3d is used in conjunction with the drag equation, [17]. The drag coefficient and reference area matrices of the quadrotor are be given by,

C_D=diag(0.2,0.22,0.5), A_D=diag(0.0907,0.0907,0.4004)m^2

The torque due to wind is found by assuming that the disturbance force is applied at $0.04\mathbf{e}_3$. All simulations were conducted using fixed-step integration with dt=$1{\cdot}10^{-3}$s.

A. Geometric-NCS comparison

For this comparison, the GNCS in [1] was selected as a benchmark since it is the first quadrotor GNCSs developed directly on SE(3), it demonstrates remarkable results in aggressive maneuvers, and to validate the claims of Sect. III-B.2. The controllers use the first set of error vectors given by $\{(7), (8)\}$, and no saturation/disturbances are included, to conclude controller competence. The gains were tuned using (35) as follows. First the attitude gains were tuned for a desired pitch command of 90^o followed by tuning the position gains for a desired $\mathbf{x}_d$=$[1; 1; 1][cm]$. Tuning the attitude controller first, ensures that during the PCM, the attitude controller embedded in the position control loop will produce homogeneous control effort. Also the gains must be compliant to (12), (29). The developed controller gains are:

$$k_\omega\text{=}150, k_R\text{=}5625, \eta\text{=}0.8$$

$$k_v\text{=}59.82, k_x\text{=}894.62, a\text{=}0.5071$$

The benchmark controller [1] parameters used are:

$$k_\omega\text{=diag}(2.1720, 2.3520, 3.2760)$$

$$k_R\text{=diag}(65.16, 70.56, 98.28), k_v\text{=}38.71, k_x\text{=}375.61$$

The initial conditions (IC's) are: $\mathbf{x}(0) = \mathbf{v}(0) = {}^b\boldsymbol{\omega}(0) = \mathbf{0}_{3\times1}, \mathbf{R}(0) = \mathbf{I}$. The results are presented in Fig. 2.

Examining Fig. 2b, the effectiveness of (16a) (solid black line: 1) with respect to the benchmark controller (dashed blue line: 2) in performing attitude maneuvers is visible as Ψ converges to zero faster and with less control effort, see Fig. 2a inner plot. The position response for a command to $\mathbf{x}_d$=$[1; 1; 1][cm]$ is shown in Fig (2c,2d). It is clear that the developed position controller (24) performs equally well with the benchmark controller, see Fig. (2d). However the attitude error during the position maneuver is negotiated better by the developed position controller as Ψ converges to zero faster and with a smaller overall error, Ψ<0.078, vs Ψ<0.1198, an important prevalence. In Fig. 2a the value of, (35), is displayed for both the attitude (inner plot), and position (outer plot), maneuvers. The benchmark controller underperforms despite using more control effort, see Fig. 2a.

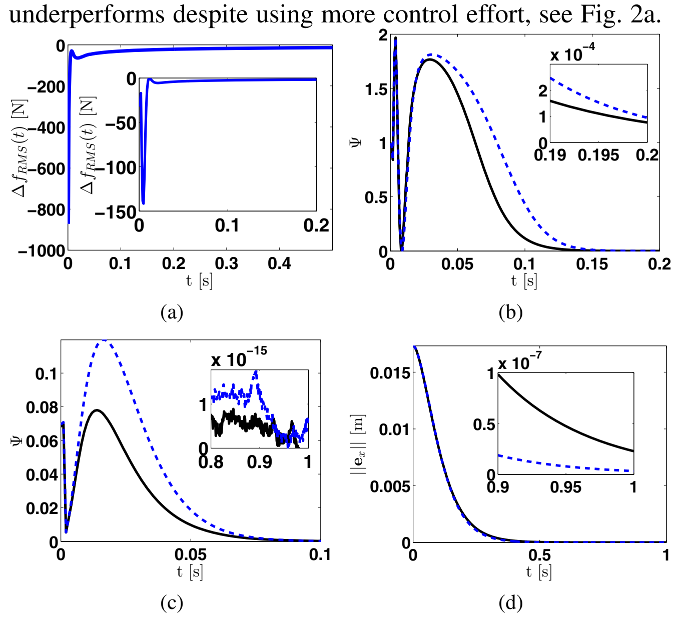

Fig. 2: Quadrotor controller comparison. (2a) RMS control effort by (35). (2b) Response for a step command of 90^o. (2c,2d) Response for a position command to $\mathbf{x}_d$=$[1; 1; 1][cm]$. (2c) Attitude error given by (7). (2d) Position error, $||\mathbf{e}_x||$. Solid lines: Developed, Dashed lines: Benchmark.

The reason that (35) exhibits large values in Fig. 2a, is due to the high gains used to achieve precise trajectory tracking. As a result because the controllers are fed with step commands, extremely large control efforts are observed.

In view of the above, the ability of the developed PCM in achieving the position command coequally to [1] but with less control effort while simultaneously negotiate the attitude error more efficiently again with less control effort makes it more effective and validates the claims of Sect. III-B.2.

B. Aggressive recovery/trajectory tracking maneuver

A complex flight maneuver is conducted, in the presence of motor saturation and noise due to wind, involving transitions between flight modes. In this simulation, the developed controllers utilize the second set of error vectors given by, $\{(9), (10)\}$. This maneuver was selected to showcase both the trajectory tracking for position and attitude, and the recovery capabilities of the developed GNCS. The IC's are: $\mathbf{x}(0) = [0; 0; 5], \mathbf{v}(0) = {}^b\boldsymbol{\omega}(0) = \mathbf{0}_{3\times1}, \mathbf{R}(0) = \mathbf{I}$. Since this simulation contains portions characterized by large error vectors, softer gains are needed to ensure smooth behavior and minimize motor saturation. The gains used are:

$$k_\omega\text{=}40, k_R\text{=}400, \eta\text{=}1.002$$

$$k_v\text{=}7.06, k_x\text{=}12.46, a\text{=}0.5081$$

The flight scenario, to be achieved through the concatenation of the two flight modes, is described next:

(a) ($t < 4$): PCM: Translation from the IC's to $\mathbf{x}_d = [0; 1; 10], \mathbf{v}_d = [0; 0; 7], \mathbf{e}_{1d} = [1; 0; 0]$ using smooth polynomials of eighth degree (SP8th).

(b) ($4 \leq t < 4.4$): ACM: The quadrotor performs a 180^o pitch maneuver, i.e. goes inverted. $\mathbf{R}_d(t)$ was designed by defining the pitch angle using $\mathrm{SP8}^{th}$.

(c) ($4.4 \leq t < 4.9$): ACM: The quadrotor recovers from its inverted state to $\mathbf{R}_d(t) = \mathbf{I}$, i.e. point to point command.

(d) ($4.9 \leq t \leq 10$): PCM: Translation to $\mathbf{x}_d = [-1; 1.5; 10], \mathbf{e}_{1d} = [1; 0; 0]$ using $\mathrm{SP8}^{th}$ with IC's equal to the states of the quadrotor at the end of the ACM.

The results of the maneuver are illustrated in Fig. 3 where the duration that the attitude mode is utilized is illustrated by the magenta colored intervals. The percentage attitude error using (9) is shown in Fig. 3a. Up to $t = 4.4$, i.e. the beginning of the quadrotor recovery from the inverted position, the atttitude error is maintained below 5% (below 9^o wrt. an axis-angle rotation). During the recovery interval ($4.4 < t < 4.9$), despite the large attitude error of 77.64% introduced by the attitude step command, the quadrotor converges to the desired orientation undeterred by the disturbances due to wind and motor saturations, see Fig. 3c, 3d. The position response is shown in Fig. 3b. During the position mode, i.e. $t<4$ and $t>4.9$, the states track the reference trajectories effectively, see Fig. 3b. At the PCM interval, $\|\mathbf{e}_x\|$ (not shown here due to space) increases above 0.06m, to 0.5m, only between $3<t<4$ where the wind increases rapidly, see Fig. 3d for the wind profile. The effect of the wind at the same interval is evident also by the noisy motor thrusts, see Fig. 3c at $3<t<4$. A simulation conducted in the absence of wind, not shown due to space, showed that the noisy behavior in Fig. 3c is eradicated and $\|\mathbf{e}_x\|<0.06$ throughout the PCM interval. Concluding, the effectiveness of the proposed GNCSs in performing precise trajectory tracking maneuvers (attitude/position) and recovery maneuvers in the presence of motor saturations and disturbances was shown. The safe switching between flight modes, stated at the end of Section III-B, was also demonstrated.

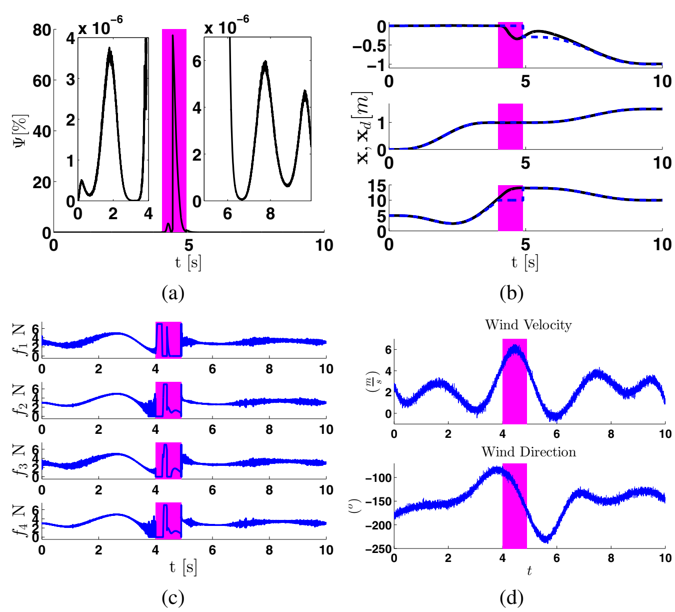

Fig. 3: Complex trajectory tracking. (3a) Attitude error given by (9). (3b) Position state $\mathbf{x}(t)$ (solid black line) and reference $\mathbf{x}_d(t)$ (blue dashed line). (3c) Thrusts (Developed). (3d) Wind profile.

V. Conclusion and Future Work

New controllers for a quadrotor UAV were developed, based on nonlinear surfaces and employing tracking errors that evolve directly on the nonlinear configuration manifold. Through rigorous stability proofs, the developed GNCS were shown to have closed-loop properties that are almost global. A region of attraction, independent of the position error, was produced and analyzed for the first time, wrt. the geometric literature. The effectiveness of the developed GNCS was validated by simulations of aggressive maneuvers, in the presence of motor saturations and disturbances due to wind.

Our future work will include experimental trials and an investigation of the developed GNCS robustness properties.

References

[1] T. Lee, M. Leok, and N.H. McClamroch, "Geometric tracking control of a Quadrotor UAV on SE(3)", in *Proc. of IEEE Conference on Decision and Control (CDC)*, 2010, pp. 5420-5425.

[2] J. Gillula, G. Hofmann, H. Huang, M. Vitus, and C. Tomlin, "Applications of hybrid reachability analysis to robotic aerial vehicles", *Int. J. Robust Nonlinear Control*, 2011, Vol 30, No. 3, pp. 335-354.

[3] D. Mellinger, and V. Kumar, "Minimum snap trajectory generation and control for quadrotors", in *Proc. of the International Conference on Robotics and Automation (ICRA)*, 2011, Shanghai, pp. 2520-2525.

[4] R. Mahony, and T. Hamel, "Robust trajectory tracking for a scale model autonomous helicopter", in *Int'l. Jrnl. of Robust and Nonlinear Control*, Vol 14, No. 12, 2004, pp. 1035-1059, DOI: 10.1002/rnc.931.

[5] P. Casau *et al.*, "Global trajectory tracking for a class of underactuated vehicles" in *Proc. of the American Control Conference (ACC)*, pp. 419-424, Washington, US, 2013.

[6] A. Abdessameud and A. Tayebi, "Global trajectrory tracking control of VTOL-UAVs without linear velocity measurements", in *Automatica*, vol. 46, pp. 1053-1059, 2010.

[7] R. Naldi *et al.*, "Robust global trajectory tracking for underactuated VTOL aerial vehicles using inner-outer loop control paradigms", *IEEE Trans. on Automatic Control*, vol. 62, no. 1, pp. 97-112, Jan 2017.

[8] T. Lee, M. Leok, and N. McClamroch, "Geometric tracking control of a Quadrotor UAV on SE(3)", *arXiv:1003.2005v1*. [Online]. Available: http://arxiv.org/abs/1003.2005v1

[9] T. Lee, "Robust Adaptive Geometric Tracking Controls on SO(3) with an Application to the Attitude Dynamics of a Quadrotor UAV", *arXiv:1108.6031*, 2011. [Onl.]. Avail.: http://arxiv.org/abs/1108.6031

[10] T. Lee, M. Leok, and N.H. McClamroch, "Non-linear robust tracking control of a quadrotor UAV on SE(3)", in *Asian Journal of Control*, 2013, vol. 15, No. 3, pp. 1-18.

[11] F.A. Goodarzi, D. Lee, and T. Lee, "Geometric Adaptive Tracking Contr. of a Quadrotor UAV on SE (3) for Agile Maneuvers", in *ASME Jrnl. of Dyn. Sys., Meas. & Contr.*, 137(9), 091007, Sep. 01, 2015.

[12] F.A. Goodarzi, D. Lee, and T. Lee, "Geometric Nonlinear PID Control of a Quadrotor UAV on SO(3)", in *Proc. of European Control Conference*, pp. 3845-3850, Zurich, Switzerland, February 2013.

[13] T. Lee, "Geometric Tracking Control of the Attitude Dynamics of a Rigid Body on $SO(3)$," in *Proceeding of the American Control Conference*, 2011, pp. 1885-1891.

[14] M. Ramp, and E. Papadopoulos, "Geometric Surface-Based Tracking Control of a Quadrotor UAV", *arXiv:1802.08920 [cs.SY]*. Available: http://arxiv.org/abs/1802.08920

[15] S. P. Bhat and D. S. Bernstein, "A topological obstruction to continuous global stabilization of rotational motion and the unwinding phenomenon," *Syst. Control Lett.*, vol. 39, no. 1, 2000, pp. 63-70.

[16] Falkenberg O. *et al.*, (2012) "Model Identification and $\mathcal{H}_\infty$ Attitude Control for Quadrotor MAV's," In: *Su CY., Rakheja S., Liu H. (eds) Intelligent Robotics and Applications. ICIRA 2012.* Lecture Notes in Computer Science, vol 7507. Springer, Berlin, Heidelberg.

[17] Batchelor, G. K., "An Introduction to Fluid Dynamics", *Cambridge University Press.* ISBN 0-521-66396-2.